Theoretical and Applied Fracture Mechanics 96 (2018) 168–173

Contents lists available at ScienceDirect

Theoretical and Applied Fracture Mechanics

journal homepage: www.elsevier.com/locate/tafmec

Fracture toughness and damage development in limpet shells

Maeve O'Neill[a], Diana Cafiso[a,b], Riccardo Mala[a], Guido La Rosa[b], David Taylor[a,*]

[a] Trinity Centre for Bioengineering, Trinity College Dublin, Ireland
[b] Department of Industrial Engineering, University of Catania, Italy

ARTICLE INFO

Keywords:
Limpet
Shell
Toughness
Fracture
Damage
Impact

ABSTRACT

Fracture toughness is an important property for many biological materials, but it can be difficult to obtain accurate and relevant values of toughness in such materials owing to complexities of geometry, material anisotropy, etc. Here we present the results of the first ever attempt to describe and measure cracking and fracture toughness in the shells of limpets. Three different experiments were devised. Firstly, small single-edge-notched bend specimens were machined, enabling us to measure K_{IC} for through-thickness cracks growing in the circumferential direction in the shell walls, giving a value of 0.98 MPa√m. Secondly, radial notches were cut into intact shells which were loaded in compression through the apex. Failure occurred by crack propagation from the notch roots, and finite element analysis (FEA) was used to obtain critical K values. However the analysis gave a surprisingly high toughness value and the results were very sensitive to test variables, especially friction. The experiment demonstrated the remarkable resistance of shells to this kind of damage, but could not be used to measure K_{IC}. Thirdly, impact tests were carried out to create internal damage in the form of delamination cracks. This allowed us to estimate toughness in terms of a crack propagation energy G_{IC} for these cracks of 146 J/m^2, equivalent to a K_{IC} of 2.59 MPa√m. Scanning electron microscopy showed that the delamination cracks had much smoother fracture surfaces than those from the through-thickness cracks, however they displayed a regular structure of folds or pleats at the 100 nm scale which may act to hinder crack face movements during shear/compression loading as occurs under impact, which is a common cause of damage for these shells in their natural surroundings.

1. Introduction

Many biological materials fail by brittle fracture in which crack-like defects propagate: examples are bone, skin and wood. This suggests that fracture toughness is an important property in determining their structural integrity. Previous workers have studied toughness and crack propagation in various natural materials, to develop better understanding of their structure/function relationships, and also to provide inspiration for the development of fracture-resistant engineering materials. Examples of previously studied materials include bone [1], cartilage [2], wood [3], eggshell [4] and insect cuticle [5]. The shells of molluscs and other marine animals have also been studied, including abalone [6], mussel [7] and conch [8]. These shells all consist of calcium carbonate plus a few percent organic material, but large differences in toughness have been found. Nacre, which constitutes one of the layers in the abalone shell, has been shown to have remarkably high toughness [9] and this had led to much biomimetic work to develop new high-toughness ceramics (e.g. [10]).

Up to now, fracture toughness has not been measured in limpet shells. Limpets live in intertidal zones in many parts of the world, being very abundant and including many different species. A significant cause of death for these animals is damage to the shell caused by impacts from moving rocks and other objects during storms [11,12]. Cracks and holes thus created may result in death by dehydration or predator attack, but limpets do have some ability to repair this damage [11]. Previously we showed that the mechanism of failure during impact is internal delamination [13]. Limpet shells consist of several layers which are laid down approximately parallel to the shell surface [14] (see Fig. 1). Impacts applied by dropping weights on the shell apex caused cracks to form on the interfaces between these layers, leading to layer separation and loss of material by spalling [13]. Another failure mode, infrequent in our work but reported as dominant in other limpet species [12], is the initiation of cracks at the shell rim and their propagation in radial and circumferential directions.

As pointed out in a recent review [15], the determination of fracture toughness for biological materials presents some particular challenges. In principle one can use approaches which are well known in the characterisation of engineering materials. Two toughness parameters

* Corresponding author at: Department of Mechanical Engineering, Trinity College Dublin, Dublin 2, Ireland.
E-mail address: dtaylor@tcd.ie (D. Taylor).

https://doi.org/10.1016/j.tafmec.2018.04.013
Received 22 February 2018; Received in revised form 30 April 2018; Accepted 30 April 2018
Available online 02 May 2018
0167-8442/

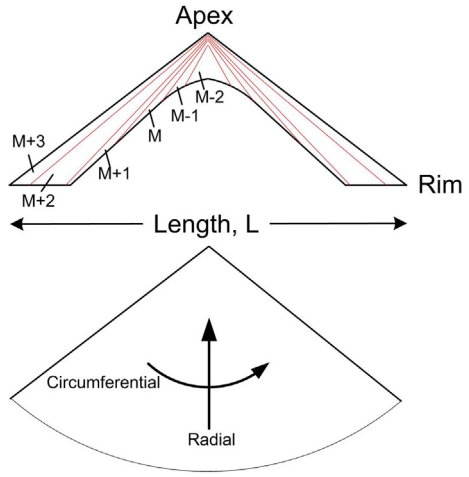

Fig. 1. Definition of the terms "apex" and "rim" and the directions "circumferential" and "radial", with respect to the limpet shell. Also shown (in schematic form) is the typical layered structure of these shells, with layers denoted M, M + 1, M − 1, etc. (adapted from Ortiz et al. [14]).

can be defined: G_c (which we will refer to as the crack propagation energy) is the amount of energy required to increase the area of the crack by a given amount, measured in J/m^2, and; K_c (the fracture toughness) allows one to calculate the stress required to cause a crack of a given length to propagate, leading to a brittle fracture. The materials concerned are almost always anisotropic and often they are available in sizes and shapes which make it difficult or impossible to obtain conventional test specimens. The aim of the present work was to determine the fracture toughness of limpet shell material, considering three different cases: through thickness cracks propagating in the radial and circumferential directions, and delamination cracks propagating between the layers within the shell thickness.

2. Methods and materials

The limpet species *Patella vulgata* (Linnaeus 1758) was chosen for study as it is present in large numbers on the coast near Dublin. Shells were obtained from living animals; using a knife it was possible to prise the shells intact and undamaged from the rocks to which they were attached. Three different experiments were devised, as illustrated schematically in Fig. 2.

2.1. Experiment 1: Circumferential propagation of through-thickness cracks

Rectangular samples of nominal dimensions 20 × 5 × 2 mm were cut and machined from the wall of the shell in the orientation shown in Fig. 2. Seven specimens were tested. Actual dimensions varied slightly and were measured using a micrometer and Vernier calipers. A sharp crack-like notch was introduced through-thickness by cutting with a fine-bladed saw and sharpening the tip with a scalpel, creating crack-like notches with root radii of approximately 5 µm and lengths (a) varying from 0.6 mm to 1 mm. These specimens were treated as conventional SENB type (single edge notched bend), loaded in three-point bend in an Instron testing machine. A typical load/displacement trace is shown in Fig. 2, indicating a clear load drop on crack propagation, which was used to calculate the fracture toughness K_C using the standard formula for a load P applied to a sample of width W, thickness B, loading span S (from ASTM E-399-83):

$$K_C = F(a/W)PS/(BW^{3/2}) \quad (1)$$

where $F(a/W) = 1.5(a/W)^{0.5}[1.99 - (a/W)(1 - (a/W))\{2.15–3.93((a/W) + 2.7(a/W)^2\}](1 + 2(a/W))^{-1}(1 - (a/W))^{-3/2}$.

2.2. Experiment 2: Radial propagation of through-thickness cracks

Intact shells were used in this experiment, tested in axial compression between steel platens (lubricated with WD40) as shown in Fig. 2. Shell rims were typically quite uneven because in the natural state they grow to conform to the rock surface. Initial experiments showed that failure tended to occur due to local stress concentrations where the rim made contact with the steel platen, so all test specimens were ground flat using silicon carbide paper. A radial notch of length 6 mm was cut in each specimen, starting at the rim, using a saw and finishing with a scalpel as in Experiment 1. Nine specimens were tested. The average rim diameter was 30.25 mm (varying from 28.5 mm to 32.5 mm). As the load trace in Fig. 2 shows, failure was associated with a sudden drop in load. For comparison purposes, a further 9 samples of similar size (varying from 26 mm to 34 mm) were tested in the same way, but without introducing a notch. A simple test was carried out to estimate the friction coefficient µ between the shell rim and the lubricated steel platen. The platen was inclined to find the angle to the horizontal at which the shell began to slide under its own weight. The value of µ is given by the tangent of this angle.

To determine the stress intensity K for this type of specimen a finite element model was created using commercial software (ANSYS Workbench 18.0). Fig. 3 shows the model and examples of results. The model was intended as a simplified version illustrating the main features of the limpet shell. It has a circular rim, whereas actual limpet shells are slightly oval in shape, and we did not include the radial ridges which are a feature of the outer surface of these shells. The outer diameter at the rim was chosen to be the same as the average experimental value (30.25 mm), whilst the height at the apex (11.88 mm) and shell wall thickness (1.29 mm except at the apex where it increases to 2.58 mm) were chosen based on published geometric data for this species [16]. A radial crack of length 6 mm (root radius zero) was included. Since the model is circular we took advantage of symmetry to model one quarter of the shell: the crack was modelled by applying boundary conditions to create a free surface over the area where the crack exists.

The mesh consisted of tetrahedral elements in most of the model, of a size sufficient to obtain three elements through thickness (which was sufficient to converge global measures such as deflection under load). In the vicinity of the crack hexahedral elements were used and the element size was refined to achieve convergence of the stress intensity result (K). The material was assumed to have a Young's modulus of 46GPa and Poisson's ratio of 0.2, based on data from the literature [17]; anisotropy of elastic modulus was not modelled for lack of information (Note: the value actually given for Patella vulgata in this source is 18GPa, however this is very much lower than all other values for related species as measured by this author, so we decided to use the average of all values for gastropod shells in this paper). Various contact states between rim and platen were considered, including fully bonded contact, and sliding with varying degrees of friction.

2.3. Experiment 3: Delamination cracking during impact testing

Impact testing was performed by placing the shell on a flat surface and dropping a cylindrical steel weight (mass 123 g, diameter 20 mm, length 50 mm) from a given height. In a previous study [13] we determined that the energy to cause failure was proportional to the shell's maximum diameter L to the power 4.6; the normalised impact strength was found to be $8.8\ MJ/m^{4.6}$. In the present work we applied impacts equal to 10% of this value to 10 shells and impacts of 20% to a further 10 shells. The shells were then cut and polished to reveal a vertical section as shown in Fig. 2. Silicon carbide papers and diamond-impregnated cloths were used, of varying roughness down to a 1 µm finish, allowing us to observe cracks in the material. Most observations were made using optical microscopy but some scanning-electron microscopy was carried out to confirm that the features being observed

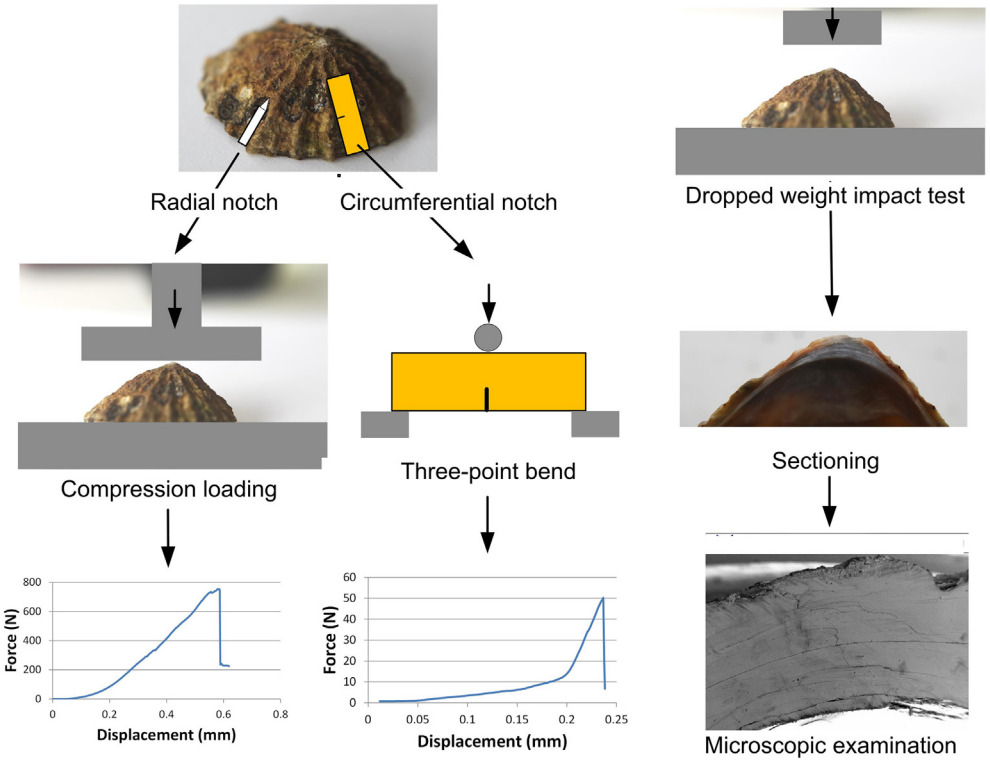

Fig. 2. Schematic illustration of the experimental plan: quasistatic toughness tests were devised for through-thickness cracks growing from notches in the radial and circumferential directions (typical force/displacement curves are shown). Impact tests were used to generate delamination cracks which were measured and counted on vertical sections.

were indeed cracks (see Figs. 2 and 4(c)) and some untested shells were examined to confirm that no damage was present. Each crack was photographed, its location noted and its length measured using image analysis software. Cracks were defined as "delamination cracks" if the entire crack lay parallel to the shell surface; the majority of cracks took this form but some deviated between layers as shown in Fig. 4(c).

It can be assumed that the vertical section chosen is typical of any such section, therefore the total area of all cracks can be calculated by assuming that every crack observed would have been visible on every section around the circumference. Thus the area of each crack observed is given by the visible length multiplied by the shell's circumference at this location. However, this calculated area will be the same, independent of our assumption about crack shape. From these results the toughness can be calculated as a crack propagation energy value G_C using the following equation:

$$G_c = \Delta U/\Delta A \tag{2}$$

where ΔU is the change in energy (in this case the difference between 10% and 20% of the critical energy, multiplied by the shell size $L^{4.6}$), and ΔA is the change in total crack area, i.e. the difference between the crack area created by impacts at 10% and at 20% of the critical energy.

However a correction is required to the above energy value, because not all the energy delivered by the impacting weight will be used to create the cracks. To find out what fraction of the delivered energy was used up in the cracking process we measured the elastic stiffness of the shells before and after impact. Fig. 5 shows an example. After impact, the force/displacement line has a smaller slope as a result of cracking: on average, the slope decreased by 27%, indicating that 27% of the delivered energy was used to create the cracks, so this correction was applied when calculating ΔU. Some energy might also be lost in irreversible processes (plastic deformation and viscoelasticity) but since the force/deflection curves were found to be relatively straight up to failure (see Fig. 2) we assumed that this was negligible.

3. Results

3.1. Experiment 1: Circumferential propagation of through-thickness cracks

The average fracture toughness K_{IC} from these tests was 0.98 MPa√m with a standard deviation of 0.23 MPa√m. Taking the Young's modulus to be 46GPa (Currey 1976) and using the formula $K = \sqrt{(GE)}$ gives a crack propagation energy G_{IC} of 21 J/m^2.

Fig. 4(a) and (b) shows typical fracture surfaces from these experiments. The fracture surfaces were macroscopically rough, consisting of several large facets at the hundred-micron scale. At high magnification, individual crystals of thickness less than 1 μm can be seen, which show smooth, flat fracture surfaces indicative of cleavage.

3.2. Experiment 2: Radial propagation of through-thickness cracks

Nine specimens were tested. All but one failed by crack propagation from the notch root, however in one case failure occurred by gradual crushing of the apex with no crack propagation. The average force to failure for the remaining 8 samples was 800.7 N (standard deviation 165 N). This was only slightly lower that the force to failure for the 9 unnotched shells (1018 N, SD 221 N) and this difference was not statistically significant (*T*-test, $p > 0.05$). The initial angle of crack propagation varied considerably, from 0° (i.e. parallel to the notch direction) to 90°, and this angle also varied considerably when viewed from inside or outside of the same shell, presumably owing the properties of the difference shell layers. The average propagation angle was 63.1° (SD 35.6°) and was similar on both outside and inside. The friction coefficient between shell and rim was measured to be 0.44 (SD 0.06).

Using the FE model we estimated the stress intensity for a given applied force, by plotting the maximum principal stress σ as a function of distance from the crack tip *r* and fitting the results to the standard formula:

$$\sigma = \frac{K}{\sqrt{2\pi r}} \tag{3}$$

However it was found that the result for K_{IC} was sensitive to the choice

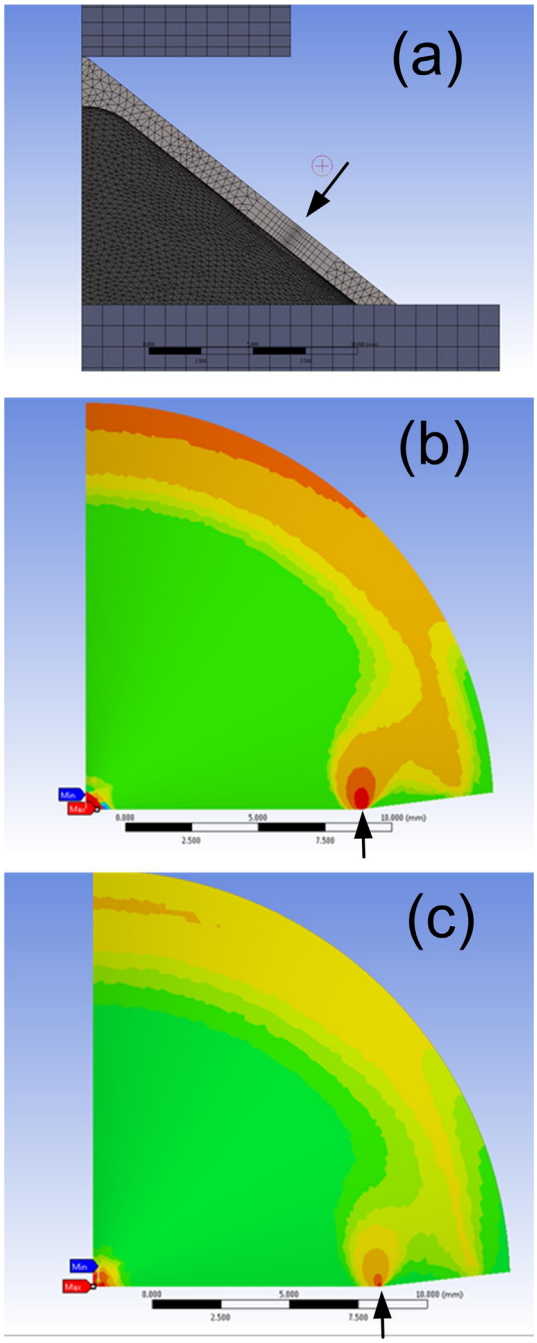

Fig. 3. (a) The finite element model, showing the quarter-model of the shell itself and the upper and lower steel platens, viewed from the side. The location of the notch tip is shown by the arrow. (b) Stress contours (viewed from above) for compressive loading at the apex with a friction coefficient μ = 0. (c) As (b) but with μ = 0.7, showing a significant reduction in notch-tip stress.

of test parameters and material properties. In particular, stresses near the crack tip were found to be strongly affected by the assumed contact condition at the rim. Assuming that the rim is fixed (i.e. bonded to the platen) gave rise to compressive stresses a short distance ahead of the crack; these stresses were even more pronounced when a Poisson's ratio of 0.3 was used. A more realistic condition of sliding with friction gave a tensile stress field (as shown in Fig. 3) but the calculated value of K was found to vary strongly with the chosen friction coefficient. Noting that cracks tended to propagate at an angle to the radial direction, we calculated K for different angles (see example images in Fig. 3 and results in Fig. 6). Stress intensity values were found to peak for angles between 45° and 90°. For our estimated friction coefficient of 0.44 the maximum stress intensity is 5.65 MPa√m (SD 1.16 MPa√m), occurring at an angle of 73° which is comparable to the experimental value of 63°. However the stress intensity value is surprisingly high: it corresponds to a crack propagation energy G_c value of 694 J/m^2 which is higher than that obtained for nacre, a shell material noted for its exceptional toughness [9].

3.3. Experiment 3: Delamination cracking during impact testing

Table 1 summarises the results from the impact testing. The 20 shells examined contained a total of 640 cracks. Even though the applied energies were only 10% and 20% of the energy to cause failure, a large number of cracks formed, and this number almost doubled when the applied energy was doubled. However the average crack length remained exactly the same at 2.7 mm, showing that the extra damage manifested itself as the formation of more cracks, rather than an increased crack length. Cracks formed predominantly in the upper third of the shell, near the apex (73–77%) rather than in the middle or lower thirds, and the great majority of cracks were delamination cracks (83–87%).

The crack propagation energy G_{IC} estimated from Eq. (2) was found to be 146 J/m^2 (standard deviation 21 J/m^2) which corresponds to a K_{IC} of 2.59 MPa√m assuming E = 46 GPa as above.

4. Discussion

Two of our three experiments were able to deliver reliable toughness values for this material. We showed that it was possible to investigate through-thickness cracking in the circumferential direction by machining small specimens of the conventional SENB type. Owing to the size and shape of the shell, especially its curvature, it was not possible to make these SENB specimens in any other orientation. Our K_{IC} value of 0.98 MPa√m is small compared to results from other types of shells. Fitzer et al. tested mussel shells using nanoindentation to obtain K_{IC} values [7]. Their results averaged about 4.5 MPa√m but showed a very large amount of scatter, varying from less than 1.0 MPa√m to more than 9.0 MPa√m. Several workers have tested nacre using through-thickness cracks in conventional fracture mechanics specimens: Currey et al. obtained a K_{IC} value of 4.5 MPa√m [6], Richter et al. found a similar value of 4.3 MPa√m [18]. Barthelat and Espinosa showed that nacre exhibits R-curve behaviour, i.e. the toughness increases with crack extension [9]. They measured G_{IC} values varying from 300 J/m^2 at crack initiation up to 1500 J/m^2 during propagation. These convert to K_{IC} values of 5.2 and 11.6 MPa√m given nacre's Young's modulus which is 90 GPa [9].

Though our K_{IC} value is much smaller, it is still considerably larger than the fracture toughness of calcium carbonate in the pure mineral form of calcite, which is 0.2–0.4 MPa√m [19,20], and also much larger than the same material in the natural form of eggshell, whose K_{IC} we measured previously as 0.3 MPa√m [4]. This implies that the microstructure of the limpet shell does confer a significant toughness increase. This microstructure is highly complex, consisting of several different layers (see Fig. 1), some of which have the calcite crystal form whilst others have the aragonite form [14]. The type and orientation of crystals varies from layer to layer. These structures, which differ in different limpet species, have been elegantly described (see for example [14]) but their role in conferring toughness has yet to be elucidated. We observed macroscopic roughness on fracture surfaces (Fig. 4(a)) which would imply some toughening as a result of crack deflection and twisting as the crack accommodates itself to the differing crystal orientations of the various layers. At the microscopic scale (Fig. 4(b)) cleavage of individual crystals was evident, which would be expected to occur at low stress intensity, but the slightly staggered appearance implies some crack deflection and frictional shearing between individual crystals during crack face separation, which may also

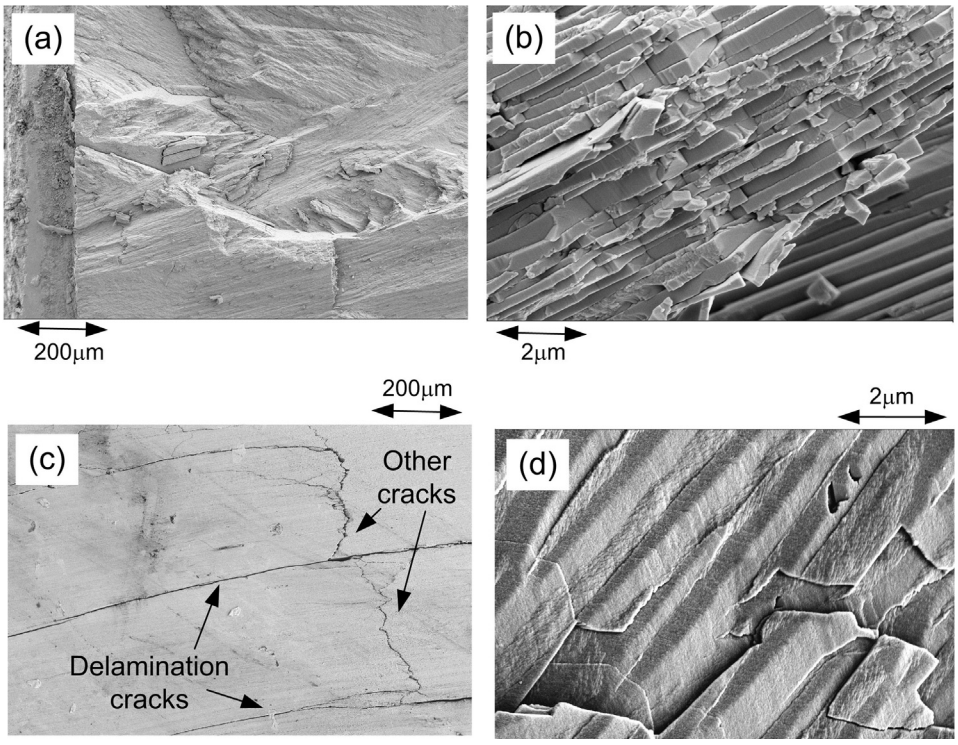

Fig. 4. Scanning electron microscope photographs: (a) The fracture surface from a circumferential crack (experiment 1: the notch is on the left hand edge), showing macroscopic roughness; (b) a higher-magnification view of part of the same surface, showing cleavage of individual crystals; (c) the polished surface from a section cut through-thickness after impact testing (experiment 3) showing typical delamination cracks and other cracks; and (d) the fracture surface from a delamination crack which was macroscopically very smooth but showed a folded appearance at high magnification.

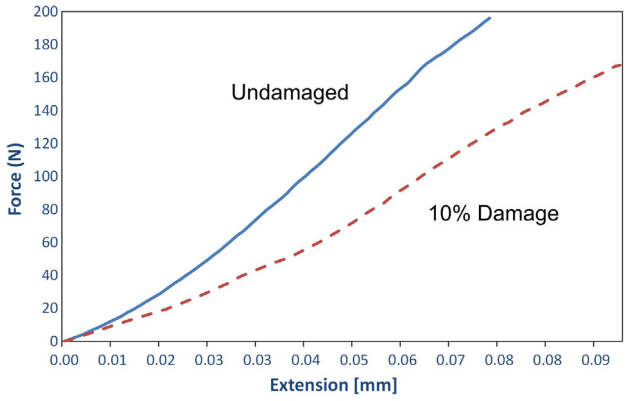

Fig. 5. Typical force/extension curves under compression loading for a shell, measured before and after receiving an impact equal to 10% of the failure energy.

Table 1
Results from impact testing.

Applied energy (% of critical)	10%	20%
Number of samples	10	10
Number of cracks per sample	24.1 (± 9.2)	39.8 (± 13.6)
Crack length	2.7 mm (± 1.8 mm)	2.7 mm (± 2.1 mm)
% of delamination cracks	87%	83%
% cracks in apex region	77%	73%
% cracks in middle region	13%	22%
% cracks in rim region	10%	5%

contribute to toughness.

Our impact tests returned a higher toughness value for delamination cracking, with G_{IC} = 146 J/m^2 and K_{IC} = 2.59 MPa√m. This result may seem surprising, because the fracture surfaces produced in these experiments were extremely smooth compared to those from the SENB specimens. However when viewed at high magnification (Fig. 4(d)) they revealed a very regular pattern of folds or pleats, which is

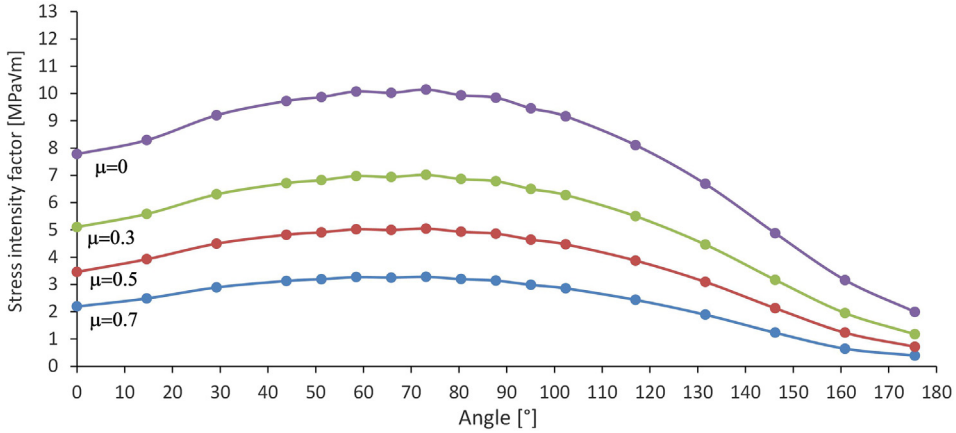

Fig. 6. Results of FEA showing stress intensity as a function of crack propagation angle and friction coefficient, for an applied compressive load equal to the average failure load of 800.7 N.

presumably a reflection of the underlying crystal structure. The roughness created by these features is only on the 100 nm scale, but it should be remembered that when these cracks are loaded by impacting the shell apex, these cracks will experience a mixture of compression and shear. Therefore these folds may lock together, hindering shear displacements between the two faces and thus reducing the shear stress intensity at the crack tips.

These values are somewhat lower than toughness values reported for nacre: 264 J/m^2 [18] and (for the initiation toughness in an R-curve) 300 J/m^2 [9], though Currey et al. measured the delamination toughness of nacre directly using chevron-notched specimens, and obtained a work-of-fracture value of 150 J/m^2, very similar to our result [6]. Failure by delamination is a common problem for materials which are built up in layers, not only natural materials but also engineering materials such as composite laminates, which also show delamination during impact tests [21]. The need to understand delamination and other failure modes which occur during impact situations has been recognised recently in a biomimetic material inspired by the conch shell structure [22].

One of our three experiments was found to be less credible as a means for generating a fracture toughness value. Whilst we were able to generate crack propagation and failure by compressing whole shells containing radial cracks, FE analysis gave a surprisingly high value of K_{IC}. This may be due to factors which were not modelled: for example these shells have surface ridges oriented in the radial direction, which are visible on Fig. 2. Our FE model did not specifically include these ridges, which may play a role in stiffening the structure and reducing stress under compressive loading. In our model, the resulting value of K_{IC} was highly sensitive to test parameters (especially friction) which are difficult to measure and not entirely under our control. We did measure a friction coefficient of $\mu = 0.44$, which is a reasonable value, but this measurement was conducted at low load (the weight of the shell itself): friction coefficients are known to change with applied load, and increasing μ would lead to lower K_{IC} predictions from our FE model, which would be more realistic. Furthermore, cracks tended to deviate away from the radial direction and towards the circumferential direction, which we already investigated successfully with our SENB specimens. What these experiments did demonstrate was that the shell is remarkably resistant to cracks in this direction: the force required to cause failure was only slightly reduced when cracks several mm in length were introduced. Unnotched samples failed by collapse of the apex, as did one of the notched samples, implying competition between two different modes of failure. This suggests that the shell has developed sufficient toughness to resist damage in the form of cracks spreading upwards from the rim.

From a biological perspective, these results demonstrate some useful adaptations which help the limpet shell to survive in its environment. As noted above, fracture due to impact is a common hazard for these creatures. One consequence of impact is the creation of internal delamination cracks, which can multiply in number and spread until failure occurs by spalling, creating a hole [13]. We found that the resistance to this kind of damage is remarkably high. Another effect of impact is the creation of a crack, which most often starts at the rim and grows upwards towards the apex. We showed that the shell is also well adapted to resist propagation in this circumferential direction. However our work also revealed a potential weakness in the low toughness for radial crack propagation. This is probably a result of the way in which the shell grows and lays down successive layers, but further work would be needed to investigate this aspect.

5. Conclusions

1. Fracture toughness for through-thickness cracks propagating circumferentially in limpet shells can be measured using SENB specimens. The resulting K_{IC} value of 0.98 MPa√m is less than values measured for some other marine shells, but considerably greater than those for calcite mineral and eggshell, implying that the multilayer structure confers some toughening mechanisms.
2. Impact tests cause internal delamination cracks, revealing a weakness in the layered structure of the shell. The crack propagation toughness obtained (G_{IC} = 146 J/m^2) revealed a relatively high value, about half that of nacre which is known for its remarkable toughness. This implies that the shells are well adapted for impact resistance.
3. Attempts to measure K_{IC} for through-thickness radial cracks showed that resistance to propagation is high in this direction, but it was not possible to achieve reliable estimates owing to the sensitivity to test parameters which are difficult to control.

Acknowledgements

Thanks to Clodagh Dooley and the Advanced Microscopy Laboratory, Trinity College Dublin, for assistance with the electron microscopy, and also to Anna Boyle for assistance with the experimental work.

Appendix A. Supplementary material

Supplementary data associated with this article can be found, in the online version, at http://dx.doi.org/10.1016/j.tafmec.2018.04.013.

References

[1] R.K. Nalla, J.J. Kruzic, J.H. Kinney, R.O. Ritchie, Effect of aging on the toughness of human cortical bone: evaluation by R-curves, Bone 35 (6) (2004) 1240–1246.
[2] D.J. Adams, K.M. Brosche, J.L. Lewis, Effect of specimen thickness on fracture toughness of bovine patellar cartilage, J. Biomech. Eng. 125 (6) (2003) 927–929.
[3] S.E. Stanzl-Tschegg, D. Keunecke, E.K. Tschegg, Fracture tolerance of reaction wood (yew and spruce wood in the TR crack propagation system), J. Mech. Behav. Biomed. Mater. 4 (5) (2011) 688–698.
[4] D. Taylor, M. Walsh, A. Cullen, P. O'Reilly, The fracture toughness of eggshell, Acta Biomater. 37 (2016) 21–27.
[5] J.H. Dirks, D. Taylor, Fracture toughness of locust cuticle, J. Exp. Biol. 215 (9) (2012) 1502–1508.
[6] J.D. Currey, P. Zioupos, P. Davies, A. Casinos, Mechanical properties of nacre and highly mineralized bone, Proc. R. Soc. Lond. B 268 (1462) (2001) 107–111.
[7] S.C. Fitzer, W. Zhu, K.E. Tanner, V.R. Phoenix, N.A. Kamenos, M. Cusack, Ocean acidification alters the material properties of Mytilus edulis shells, J. R. Soc. Interf. 12 (103) (2015).
[8] Y.A. Shin, S. Yin, X. Li, S. Lee, S. Moon, J. Jeong, M. Kwon, S.J. Yoo, Y.M. Kim, T. Zhang, H. Gao, S.H. Oh, Nanotwin-governed toughening mechanism in hierarchically structured biological materials, Nat. Commun. 7 (2016).
[9] F. Barthelat, H. Tang, P.D. Zavattieri, C.M. Li, H.D. Espinosa, On the mechanics of mother-of-pearl: a key feature in the material hierarchical structure, J. Mech. Phys. Solids 55 (2) (2007) 306–337.
[10] H. Zhang, P. Shen, A. Shaga, R. Guo, Q. Jiang, Preparation of nacre-like composites by reactive infiltration of a magnesium alloy into porous silicon carbide derived from ice template, Mater. Lett. 183 (2016) 299–302.
[11] G.C. Cadee, Shell damage and shell repair in the Antarctic limpet Nacella concinna from King George Island, J. Sea Res. 41 (1–2) (1999) 149–161.
[12] A.L. Shanks, W.G. Wright, Adding teeth to wave action: the destructive effects of wave-borne rocks on intertidal organisms, Oecologia 69 (3) (1986) 420–428.
[13] D. Taylor, Impact damage and repair in shells of the limpet Patella vulgata, J. Exp. Biol. 219 (2016) 3927–3935.
[14] J.E. Ortiz, I. Gutierrez-Zugasti, T. Torres, M. Gonzalez-Morales, Y. Sanchez-Palencia, Protein diagenesis in Patella shells: implications for amino acid racemisation dating, Quat. Geochronol. 27 (2015) 105–118.
[15] D. Taylor, Measuring fracture toughness in biological materials, J. Mech. Behav. Biomed. Mater. 77 (2018) 776–782.
[16] J.P. Cabral, R.M. Natal Jorge, Compressibility and shell failure in the European Atlantic patella limpets, Mar. Biol. 150 (4) (2007) 585–597.
[17] J.D. Currey, Further studies on the mechanical properties of mollusc shell material, J. Zool. Soc. Lond. 180 (1976) 445–453.
[18] B.I. Richter, S. Kellner, H. Menzel, P. Behrens, B. Denkena, S. Ostermeier, C. Hurschler, Mechanical characterization of nacre as an ideal-model for innovative new endoprosthesis materials, Arch. Orthop. Trauma Surg. 131 (2) (2011) 191–196.
[19] J. Lv, Y. Jiang, D. Zhang, Structural and mechanical characterization of atrina pectinata and freshwater mussel shells, J. Bionic Eng. 12 (2) (2015) 276–284.
[20] M.E. Broz, R.F. Cook, D.L. Whitney, Microhardness, toughness, and modulus of Mohs scale minerals, Am. Mineral. 91 (1) (2006) 135–142.
[21] K. Azouaoui, Z. Azari, G. Pluvinage, Evaluation of impact fatigue damage in glass/epoxy composite laminate, Int. J. Fatigue 32 (2) (2010) 443–452.
[22] G.X. Gu, M. Takaffoli, M.J. Buehler, Hierarchically enhanced impact resistance of bioinspired composites, Adv. Mater. 29 (28) (2017).